Barium vanadium silicate $BaVSi_2O_7$: A t_{2g} counterpart of the Han purple compound

A. Vasiliev,[1] O. Volkova,[1] E. Zvereva,[1] M. Isobe,[2] Y. Ueda,[2] S. Yoshii,[3] H. Nojiri,[3] V. Mazurenko,[4] M. Valentyuk,[4,5] V. Anisimov,[4,6] I. Solovyev,[4,7] R. Klingeler,[8] and B. Büchner[9]

[1]*Low Temperature Physics and Superconductivity Department, Lomonosov Moscow State University, 119991 Moscow, Russia*
[2]*Materials Design and Characterization Laboratory, Institute for Solid State Physics, University of Tokyo, Kashiwa 277-8581, Japan*
[3]*Institute for Materials Research, Tohoku University, Sendai 980-8577, Japan*
[4]*Theoretical Physics and Applied Mathematics Department, Ural Federal University, 620002 Ekaterinburg, Russia*
[5]*Institute for Theoretical Physics, University of Hamburg, 20355 Hamburg, Germany*
[6]*Institute of Metal Physics, Russian Academy of Sciences, 620990 Ekaterinburg, Russia*
[7]*Computational Materials Science Unit, National Institute for Materials Science, Tsukuba 305-0047, Japan*
[8]*Kirchoff Institute for Physics, Heidelberg University, 69120 Heidelberg, Germany*
[9]*Leibniz Institute for Solid State and Materials Research, IFW Dresden, 01171 Dresden, Germany*

(Received 11 October 2012; revised manuscript received 25 March 2013; published 11 April 2013)

By means of thermodynamic and magnetic resonance measurements the $S = 1/2$ dimer system $BaVSi_2O_7$ is characterized. A broad maximum in the temperature dependence of the magnetic susceptibility and a Schottky-type anomaly in the specific heat allows estimating the main exchange interaction within V^{4+}-V^{4+} dimers as $J = 37 \pm 1$ K. This estimation is confirmed by pulsed magnetic field measurements of the magnetization, which is evidenced by the field-induced singlet-triplet transition at about 27 T. Both X-band and high-field terahertz electron spin resonance data qualitatively agree with the results of the specific heat and magnetization measurements. The electronic structure calculations, by using local density approximation, indicate that the magnetic properties of $BaVSi_2O_7$ can be interpreted within the weakly interacting dimer model.

DOI: 10.1103/PhysRevB.87.134412 PACS number(s): 75.40.Cx, 76.30.−v

I. INTRODUCTION

The quantum ground states of low-dimensional magnetic systems differ principally from those in their three-dimensional counterparts. In some cases, the quantum ground states of low-dimensional magnets are characterized not only by the absence of long-range magnetic order but in addition by vanishing magnetization at low temperatures due to an energy gap in the spectrum of magnetic excitations. In particular, the spin-gapped systems are dimers,[1] plaquettes,[2] alternating chains,[3] and even-leg spin ladders.[4,5] Similar states are realized[6] or presumed[7] in some topologies of 2D Heisenberg magnets. The absence of long-range magnetic order is a sequence of low dimensionality and/or frustration and does not mean lack of exchange interaction, which can be comparable to that in three-dimensional systems.

By means of external magnetic field, it is possible to overcome the gap and to drive the system from its nonmagnetic ground state to a magnetic one, even at low temperatures. The spin-gap state is suppressed when the Zeeman interactions appear to be comparable to the scale of magnetic interactions.[8] The quantum nature of ground states in low-dimensional magnets can reveal itself, e.g., in the appearance of fractional plateaus in the magnetization at low temperatures.[6] A famous example of a spin-gap system is the ancient pigment $BaCuSi_2O_6$, the so called Han purple compound, in which the electronic properties are governed by magnetically active e_g orbitals.[9] Here, the spin gap can be closed by external magnetic fields, thereby creating interacting bosonic triplon excitations, and magnetically induced Bose–Einstein condensation of triplons is observed. In the present work, the thermodynamic and resonant properties of the t_{2g} counterpart of the Han purple compound, i.e., $BaVSi_2O_7$, were studied both experimentally and theoretically.

II. CRYSTAL STRUCTURE

The $BaVSi_2O_7$ structure is shown in Fig. 1. The second phase ß-$BaVSi_2O_7$ (hereafter named $BaVSi_2O_7$) crystallizes in the tetragonal space group $I4/m$ (No. 87), with $a = 7.0535(7)$ Å, $c = 11.467(2)$, $V = 570.5(3)$ Å^3, and $Z = 4$ (Ref. 10). This structure can be considered as consisting of $[VO_5]^{6-}$ square pyramids and unbranched single rings of $[Si_4O_{12}]^{8-}$, or of cage-like $[Si_4V_2O_{18}]^{12-}$ clusters formed by $[SiO_4]^{4-}$ and $[VO_5]^{6-}$. These building elements are cross-linked to form a pseudo-two-dimensional (2D) network containing empty channels perpendicular to the c axis (cf. Fig. 1, left panel). The 2D networks are held together by Ba^{2+} ions that occupy channels parallel to the c axis. The magnetically active cations V^{4+} ($3d^1$, $S = 1/2$) are in a distorted pyramidal oxygen environment. There are four basal oxygen ions at a distance of 1.936 Å and one apical oxygen ion at a distance of 1.593 Å from the central vanadium ion in the VO_5 pyramid. One may presume that the magnetically active orbital is the d_{xy} orbital of the V ion. The VO_5 pyramids constitute bipyramidal dimers via silicate groups SiO_4 attached to every basal oxygen ion (cf. Fig. 1, right panel). The magnetic exchange interaction within these dimers J_d is presumably organized through V-O-O-O-V pathways. The distance between V^{4+} ions within a dimer amounts to 3.594 Å. The complexes of vanadium dimers consisting of two VO_5 pyramids and four SiO_4 tetrahedra are interconnected via vertices of silicate groups forming a 2D bilayer square lattice. The distance between vanadium ions in neighboring dimers is 7.053 Å. On the other hand, neighboring bilayers are shifted with respect to each other for the half-period so that the shortest distance between vanadium ions in neighboring bilayers is 5.43 Å. However, there is no evident magnetic pathway transferring the exchange interaction between neighboring bilayers.

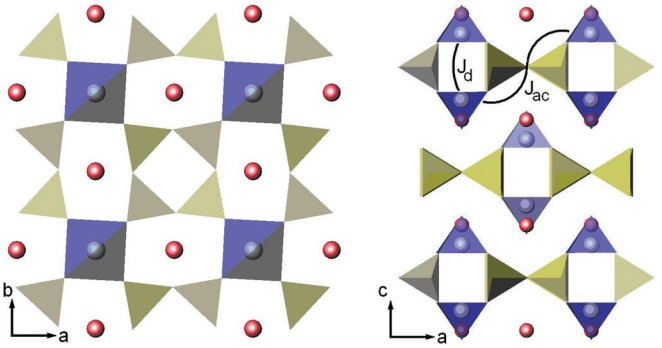

FIG. 1. (Color online) The crystal structure of $BaVSi_2O_7$ (cf. Ref. 10). Left panel: the intralayer topology; right panel: the interlayer arrangement. The apparent square and triangular polyhedra represent VO_5 pyramids and SiO_4 tetrahedra, respectively. Ba^{2+} ions (circles) occupy the interlayer. The arcs J_d and J_{ac} denote intradimer and interdimer exchange pathways, respectively.

III. EXPERIMENTAL

The powder sample of $BaVSi_2O_7$ was synthesized by a solid-state reaction of mixtures with an appropriate molar ratio of $BaSiO_3$, V_2O_5, V_2O_3, and SiO_2. The weighed mixtures were pressed into pellets and heated at 1100 °C in an evacuated silica tube for several days. The $BaSiO_3$ was prepared by heating mixtures of $BaCO_3$ and SiO_2 at 900 °C in air. The prepared sample was checked by means of x-ray diffractometer (Radian), Cu K_α radiation. The temperature dependence of the magnetic susceptibility of $BaVSi_2O_7$ was measured in the range 2–350 K by means of a Magnetic Property Measurement System (MPMS) 5 T (Quantum Design). The field dependence of the magnetization up to $B = 30$ T, at $T = 1.6$ K, was measured in a pulsed magnetic field by an inductive method and calibrated using the low-magnetic-field data. Low-field electron spin resonance (ESR) studies were carried out using an X-band ESR spectrometer CMS 8400 (ADANI) ($f \approx 9.4$ GHz, $B \leqslant 0.7$ T) equipped with a low-temperature mount, operating in the range $T = 6$–270 K. The effective g-factor of vanadium ions in $BaVSi_2O_7$ has been calculated with respect to *a,g*-bisdiphenyline-*b*-phenylallyl, $g_{et} = 2.00359$, as reference material. High-field ESR measurements have been performed at 135, 190, and 405 GHz and in pulsed magnetic fields up to 30 T. Details of the terahertz ESR system are given in Ref. 11. The temperature dependence of specific heat in $BaVSi_2O_7$ was measured by means of a relaxation method in a Physical Property Measurement System (PPMS) 9 T (Quantum Design).

IV. MAGNETIC SUSCEPTIBILITY

The temperature dependence of the magnetic susceptibility $\chi = M/B$ in $BaVSi_2O_7$ measured at $B = 0.1$ T is shown in Fig. 2. At high temperatures, the χ vs T dependence follows the Curie–Weiss law,

$$\chi = \chi_0 + \frac{C}{T - \Theta}, \tag{1}$$

where $\chi_0 = -2.0 \times 10^{-5}$ emu/mol is a temperature-independent term, $C = 3.4 \times 10^{-1}$ emu K/mol is the Curie constant, and $\Theta = -9.2$ K is the Weiss temperature, as

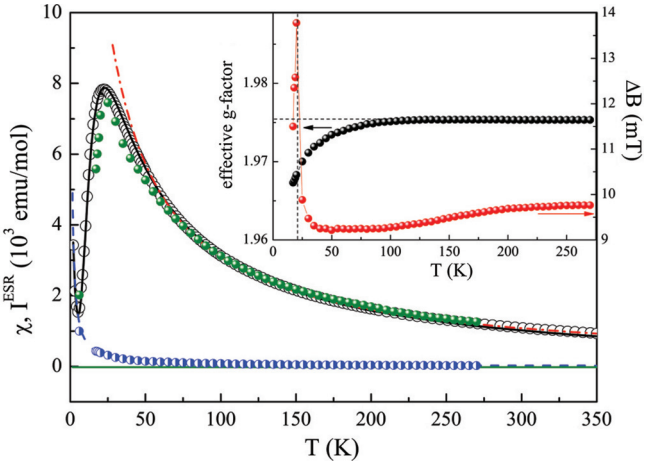

FIG. 2. (Color online) Temperature dependencies of the static magnetic susceptibility χ (open circles) and the integral ESR intensity I^{ESR} (closed circles) (see the text). The dash dotted line is the Curie–Weiss fit of the static magnetic susceptibility extrapolated from high temperatures; the dashed line is the impurity/defect Curie contribution χ_{imp}, and the half-filled circles superimposed on this line show the impurity/defect contribution as extracted from the X-band ESR data. The horizontal line at negative values of χ represents the temperature-independent contribution χ_0; the solid line displays the fit of the experimental data in the whole range of temperatures. The inset represents the linewidth ΔB and the effective g-factor vs temperature for the main component of the X-band ESR spectra.

found from the fit in the range 200–300 K. The temperature-independent term comprises the diamagnetic contributions of all ions and the paramagnetic van Vleck contribution of the vanadium ions. The former can be estimated from Pascal's constants[12] to $\chi_{dia} = -1.2 \times 10^{-4}$ emu/mol, and a van Vleck contribution of $\chi_{vV} = 1.175 \times 10^{-4}$ emu/mol is obtained from the simplified formula[13]

$$\chi_{vV} = \frac{4N_A\mu_B^2}{\Delta E}, \tag{2}$$

where N_A is the Avogadro number, μ_B is the Bohr magneton, and ΔE is the energy gap between the occupied d_{xy} orbital and the empty d_{xz}/d_{yz} orbitals in the V^{4+} d shell (cf. Table I). The experimentally found Curie constant C gives a somewhat reduced value of the squared effective magnetic moment as $2.7\mu_B^2$ compared with the spin-only value of $p^2 = 3.0\mu_B^2$. The value of the Weiss temperature Θ allows estimating the main exchange interaction parameter according to the mean field formula

$$\Theta = \frac{zS(S+1)}{3k_B}J, \tag{3}$$

where $z = 1$ is the number of nearest neighbors of the magnetically active V^{4+} ions in the $BaVSi_2O_7$ crystal structure, S is the

TABLE I. The energies of the Wannier orbitals obtained using the projection procedure (in eV).

xy	yz	$3z^2 - r^2$	xz	$x^2 - y^2$
0	1.1	2.3	1.1	2.5

spin, and k_B is Boltzmann's constant. Applying to this analysis and the experimentally obtained Weiss temperature the value of the leading exchange interaction parameter J within the dimers of V^{4+}, $S = 1/2$ amounts to 37 K.

At cooling, the $\chi(T)$ curve deviates from the Curie–Weiss law, passes through a broad maximum at $T_{max} = 23$ K, and drops rapidly. At the lowest temperatures, there is an upturn of χ that can be ascribed to the presence of defects/impurities in the sample. In the whole temperature range studied, magnetic susceptibility can be described by the sum of a temperature-independent term χ_0, an impurity term χ_{imp} that follows the Curie law, and the dimer contribution χ_{dim}, which can be well described in terms of noninteracting dimers:

$$\chi = \chi_0 + n\frac{N_A g_{imp}^2 S(S+1)\mu_B^2}{3k_B T} + (1-n)\frac{N_A g_{dim}^2 \mu_B^2}{k_B T}\frac{1}{\left[3+\exp\left(\frac{J}{k_B T}\right)\right]}. \quad (4)$$

Here, $n = 0.02$ is the defect/impurity concentration, $g_{imp} = 1.95$ is the g-factor of the defects/impurities, $g_{dim} = 1.975$ is the g-factor of the vanadium ions forming the magnetic dimers as derived from the X-band ESR measurements. The antiferromagnetic exchange interaction parameter within the V^{4+}-V^{4+} dimers amounts to $J = 38$ K, which nicely coincides with the value found within the high-temperature fitting procedure.

V. ELECTRON SPIN RESONANCE

Low-field ESR data corroborate well the static magnetization data. The evolution of the X-band ESR spectra with temperature for a powder sample of $BaVSi_2O_7$ is presented in Fig. 3. The signal intensity increases upon decreasing temperature, passes through a maximum at about 30 K, and then decreases upon further cooling. The shape of the ESR line changes in the low-temperature range, and a partly resolved hyperfine structure appears below 20 K. At 6 K, eight equidistant components superimposed over a broad central line may be inferred, which is a sign of the hyperfine structure originating from the interaction between the electron magnetic moment of the unfilled electron shell of V^{4+} ions and the nuclear magnetic moment of the ^{51}V isotope ($I = 7/2$, natural abundance 99.76%). The hyperfine interaction constant ^{51}A was estimated to be about 200 MHz.

The lineshape can be satisfactorily analyzed by a standard Lorenzian function,

$$\frac{dP}{dB} \propto \frac{d}{dB}\left[\frac{\Delta B}{\Delta B^2 + (B - B_r)^2}\right], \quad (5)$$

where P is the power absorbed in the ESR experiment, B is the magnetic field, B_r is the resonance field, and ΔB is the linewidth. However, the proper description of the ESR spectra requires including two spectral components: a main contribution to the absorption line that is at least 10 orders of magnitude more intensive than an additional weak line, probably related to a small amount of paramagnetic impurities, as also inferred from the static magnetization data. Results of ESR lineshape fitting by the sum of two Lorenzians [Eq. (5)] are shown by solid lines in Fig. 3. Apparently, the fitted curves are in excellent agreement with the experimental data.

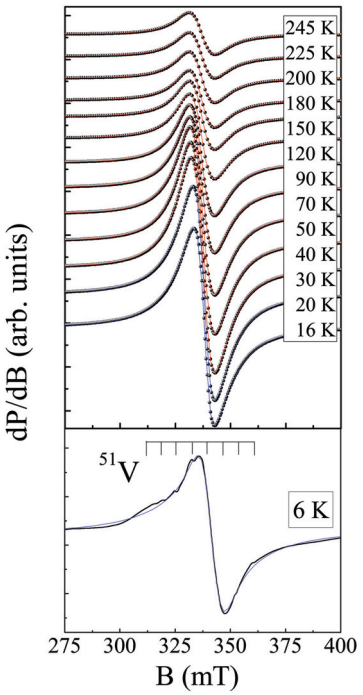

FIG. 3. (Color online) Temperature evolution of the first derivative X-band absorption for powder sample $BaVSi_2O_7$ sample: points are experimental data; solid lines are the result of fitting by sum of two Lorenzians in accordance with Eq. (2). The spectra are shifted with respect to each other for clarity.

The main ESR signal from the dimer system in the paramagnetic phase is characterized by a temperature-independent effective g-factor, $g = 1.975 \pm 0.005$. However, there is a marked shift of the resonant field to higher magnetic fields below ~70 K, indicating an increased role of magnetic fluctuations; i.e., the shift signals the short-range ordering regime. The linewidth decreases slowly upon lowering of the temperature, remains practically constant in the range from 100 K down to 35 K, and eventually broadens again. Upon further decrease of the temperature, the linewidth abruptly grows, to maximum at T_{max}, and then decreases again below T_{max}. The broadening of the signal and concomitant deviation from the Lorenzian profile is a signature of suppression of the exchange-narrowing effect due to the slowing down of the spin-spin correlations by approaching the short-range ordering regime. The intensity of the ESR resonance lines is known to be proportional to the number of paramagnetic spins. We have estimated the full area under the absorption line by double integration of the first derivative ESR spectrum for each temperature. The temperature dependence of the integral ESR intensity $I^{ESR}(T)$ (closed circles in Fig. 2) agrees quite well with the static magnetic susceptibility data $\chi(T)$. At elevated temperatures, the ESR response is dominated by the dimer spins, which are thermally activated.[14] The data hence confirm the intrinsic nature of the spin-gap behavior of the dimer contribution. The characteristic effective g-factor ($g = 1.950 \pm 0.005$) corresponding to the weaker line is almost temperature independent over the entire range of the

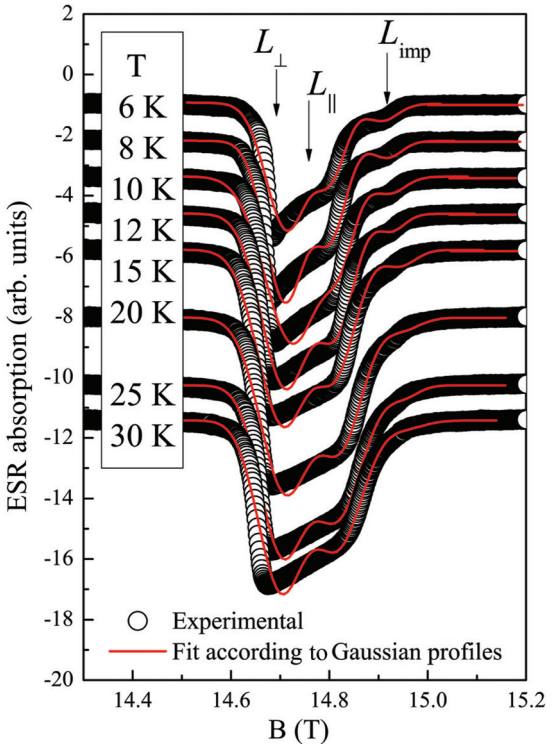

FIG. 4. (Color online) Evolution of the ESR spectra with temperature at 405 GHz for powder sample $BaVSi_2O_7$: the circles are experimental data; lines are the results of fitting according to Gaussian lineshape profile [Eq. (3)]. The spectra are shifted with respect to each other for clarity.

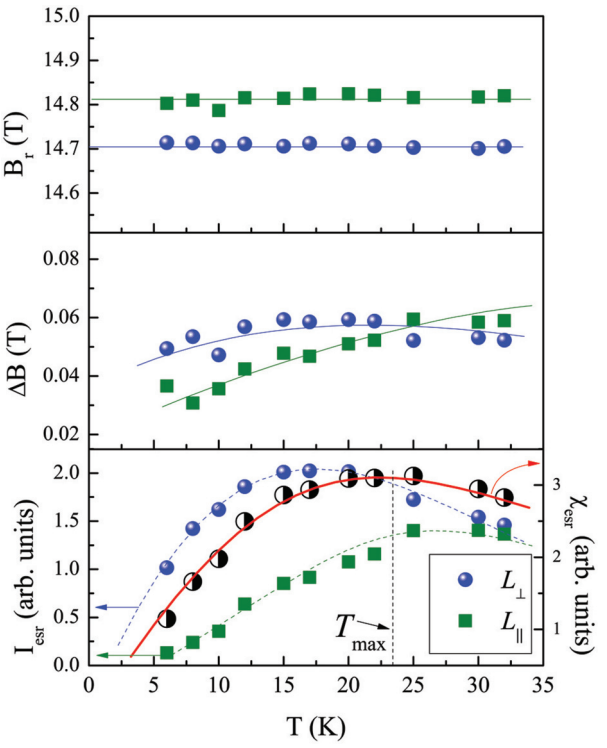

FIG. 5. (Color online) Temperature dependence of the resonance field (upper panel), the linewidth (middle panel), and the integral ESR intensity (lower panel) derived from the fitting of transmission spectra at 405 GHz according to Eq. (3) for powder sample $BaVSi_2O_7$.

temperature variation, but the integral ESR intensity increases noticeably in the low temperature range in accordance with the Curie–Weiss law (half-filled circles in Fig. 2).

In contrast to the low-field X-band ESR data, where the mean ESR signal from the dimer subsystem is exchange-narrowed into a single Lorenzian line, the high-field ESR spectra taken at terahertz frequencies f up to 405 GHz in the low temperature range (4.2–35 K) allow one to resolve the anisotropic magnetic interactions in more details. The most striking results obtained from the high-field ESR data are collected in Figs. 4–6. The $f(B)$ dependence at 4.2 K demonstrates a linear gapless character typical for the paramagnetic state (left lower panel in Fig. 6). Its extrapolation to low fields intersects the origin and matches very well with the measurements at $f = 9.5$ GHz with a g value of about 1.975. When increasing the frequency, and consequently the required magnetic field for the resonance condition, we observe a gradual deviation of the detected line from an exchange-narrowed Lorenzian shape to a strongly anisotropic resonance line. While at $f = 135$ GHz the transmission spectrum can be described equally well by both the sum of two Lorenzians and two Gaussians, at higher frequencies, the ESR lineshape changes toward a clear Gaussian form. Hence, two ($f = 190$ GHz) or even three ($f = 405$ GHz) Gaussian profiles should be used for an analysis of the spectra (as an example, see the red solid curves for fitting by Gaussians and the blue curve for fitting by Lorenzians in Fig. 6).

A representative example of the high-field ESR data analysis is given in Figs. 4 and 5 for transmission spectra taken at 405 GHz. For the quantitative estimations we used a standard Gaussian function,

$$\frac{dP}{dB} \propto \frac{d}{dB}\left[\exp\left(\frac{(-\ln 2)(B - B_r)^2}{\Delta B^2}\right)\right] \qquad (6)$$

where P, B, B_r, ΔB denote the same quantities as explained above for Eq. (5). Results of lineshape fitting by the sum of three Gaussians [Eq. (6)] are shown by red solid curves in Fig. 4. In addition, an example of spectrum decomposition along with the three resolved lines is given in the upper panel of Fig. 6 (constituting inclined pattern $L_\perp$, vertical pattern L, and horizontal pattern L_{imp} resonance modes, respectively, while the solid line displays their sum). The fitting curves give a reasonable description of the transmission spectra. Presumably, the two main components, L and $L_\perp$, of the spectra originate from the vanadium dimer subsystem reflecting approximately 2% anisotropy of the g-factor of the V^{4+} ions in a pyramidal environment, while similar to the X-band ESR data, a weak additional line L_{imp} at the right shoulder of the resonance line originates from the impurities/defects. The increase of the role of magnetic anisotropy below T_{max} suppresses the exchange-narrowing effect and allows observing both resonance modes in high magnetic fields corresponding to two principal components, parallel g and perpendicular $g_\perp$, of the g-tensor for the powder spectrum of $BaVSi_2O_7$. In higher fields, the lowest branch of the excited triplet splits due to the Zeeman effect, and the gap between the singlet and the lowest branch of the triplet reduces to 60% of the one observed at zero field.

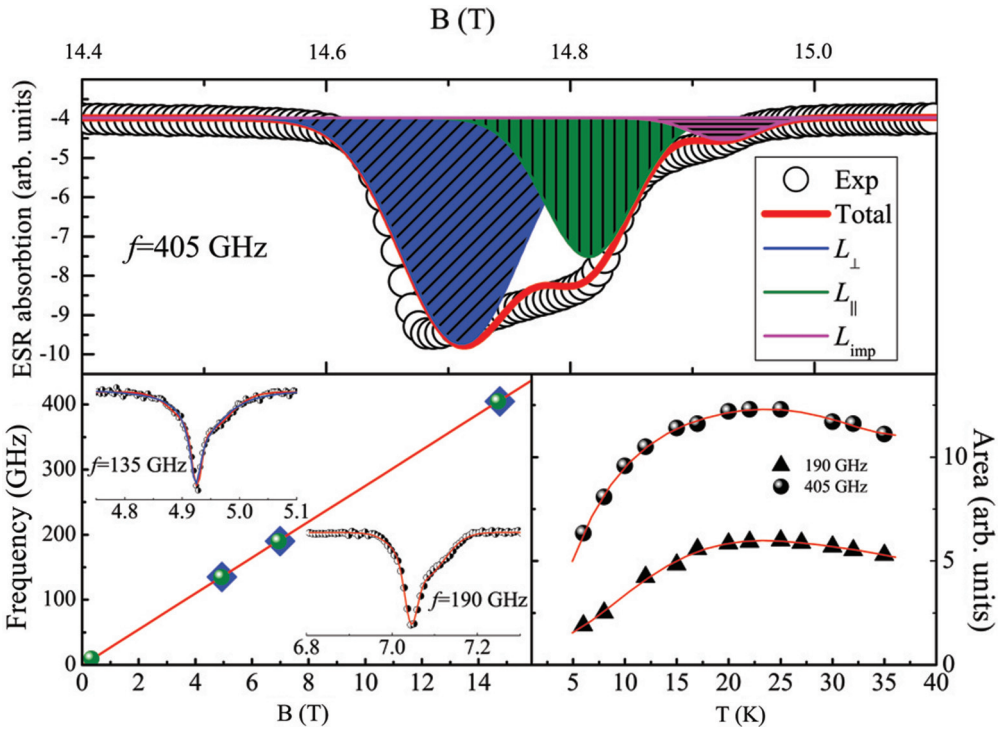

FIG. 6. (Color online) Upper panel: a representative example of the ESR spectrum decomposition along with three resolved absorption lines (constituting inclined pattern $L_\perp$, vertical pattern L, and horizontal pattern L_{imp} resonance modes, respectively, while the solid line displays their sum). Lower panel: (left) the resonance frequencies vs magnetic field plot and representative transmission spectra at 135 GHz and 190 GHz, respectively (circles are experimental data; lines are the results of fitting, as described in text); (right) the temperature dependence of the ESR absorption area at 190 GHz and 405 GHz.

The temperature dependences of the ESR parameters (the resonance field, linewidth, and integral ESR intensity) for the two principal components of the anisotropic spectra derived by fitting according to Eq. (6) are shown in Fig. 5. Apparently, the resonance field remains temperature independent for all temperatures (upper part of Fig. 5). The parallel component slightly narrows with decreasing temperature, whereas the linewidth of the perpendicular component weakly varies with temperature (middle part of Fig. 5). At the same time, the integral ESR intensity clearly shows the evolution of short-range spin correlations, which is indicated by the broad maximum for both components (circles and squares on lower panel of Fig. 5). The total integral ESR intensity χ_{esr} (i.e., the sum of both main components) nicely follows the static magnetic susceptibility with a smooth maximum at around $T_{max} \sim 23$ K (half-filled circles in the lower panel of Fig. 5 and circles and triangles in the right lower panel on Fig. 6).

VI. HIGH-FIELD MAGNETIZATION

The field dependence of magnetization in $BaVSi_2O_7$ taken in a pulsed magnetic field at 1.6 K is shown in Fig. 7. The main feature is the rapid increase of magnetization at $B_C = 27.2$ T, as given by the maximum of the derivative, below which saturation is nearly reached. This feature signals the transition to the triplet state, i.e., breaking of the intradimer bonds by the external magnetic field. The exchange interaction parameter estimated from the value of the critical field amounts to $J = g\mu_B B_C = 36$ K, which agrees with the value estimated from the temperature dependence of the magnetic susceptibility. At low fields, the magnetization curve is slightly right-bended, indicating a small Brillouin-like contribution due to quasi-free impurity spins.

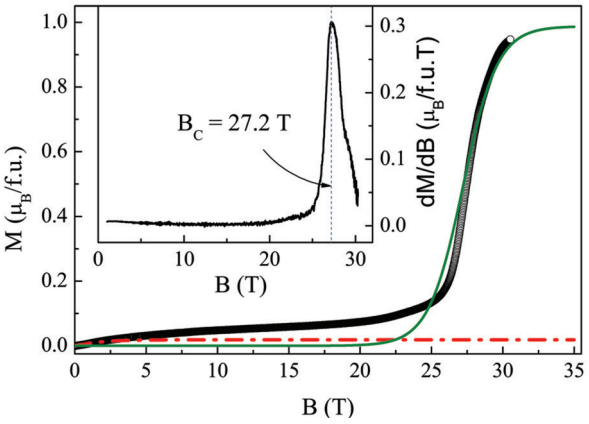

FIG. 7. (Color online) The magnetization curve of $BaVSi_2O_7$ at 1.6 K. The defect/impurity contribution approximated by the Brillouin function is shown by the dash-dotted line. The solid line represents the fit of the $M(B)$ curve in a noninteracting dimer model. The inset represents the derivative of the magnetization curve; the critical magnetic field $B_C = 27.2$ T is indicated by the vertical dashed line.

The $M(B)$ dependence can be fitted by means of the noninteracting dimer model according to the formula

$$M = \frac{g\mu_B}{Z}\left[\exp\left(-\frac{J - g\mu_B B}{k_B T}\right) - \exp\left(-\frac{J + g\mu_B B}{k_B T}\right)\right], \tag{7}$$

where the partition function Z is given by the expression

$$Z = 1 + \exp\left(-\frac{J - g\mu_B B}{k_B T}\right) + \exp\left(-\frac{J}{k_B T}\right) + \exp\left(-\frac{J + g\mu_B B}{k_B T}\right). \tag{8}$$

The curve fit at $T = 1.6$ K with $J = 36$ K and $g = 1.975$ is shown by the solid line in Fig. 7. Evidently, at intermediate fields ($B < B_C$), the experimentally observed magnetization significantly exceeds the defects/impurities, as well as the dimer contributions, in the noninteracting dimer model. Tentatively, interdimer exchange interactions may lead to excess magnetization in $BaVSi_2O_7$ at values of $B < B_C$ seen in pulsed magnetic field measurements.

VII. SPECIFIC HEAT

The analysis of static and dynamic magnetic properties given above is strongly confirmed by the temperature dependence of the specific heat in $BaVSi_2O_7$, shown in Fig. 8. Evidently, there is significant extra contribution to the specific heat at low temperatures, compared with the specific heat in the isostructural nonmagnetic counterpart $BaTiSi_2O_7$. This extra contribution can be ascribed to the Schottky-type anomaly related to singlet-triplet excitations in the V^{4+}-V^{4+} dimers, as

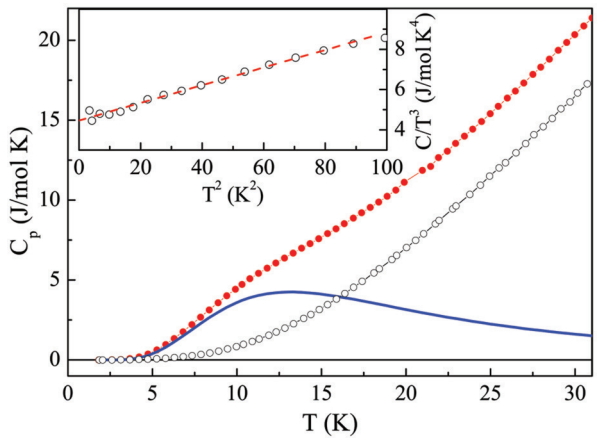

FIG. 8. (Color online) The temperature dependencies of the specific heat, C_p, of $BaVSi_2O_7$ and its isostructural nonmagnetic counterpart $BaTiSi_2O_7$ are shown by solid and open circles, respectively. The singlet-triplet magnetic excitation contribution in the V^{4+}-V^{4+} dimers C_{dim}, calculated by means of Eq. (7) with $J = 37$ K, is shown by the solid line. The inset represents the specific heat of $BaTiSi_2O_7$ on a C/T^3 vs T^2 scale; the dashed line represents a Debye fit to the data.

given by the formula

$$C_{dimers} = \frac{3}{2}R\left(\frac{J}{k_B T}\right)^2 \frac{\exp\left(-\frac{J}{k_B T}\right)}{\left[1 + 3\exp\left(-\frac{J}{k_B T}\right)\right]^2}, \tag{9}$$

where R is the universal gas constant and $J = 38$ K. While it is not reliable to estimate the Debye temperature of $BaVSi_2O_7$ from the low-temperature fitting procedure, it can be done for $BaTiSi_2O_7$. The inset to Fig. 8 represents C/T^3 vs T^2 dependence, which corresponds to Debye model

$$C_{lat} = \beta T^3 + \delta T^5 \tag{10}$$

with $\beta = 4.5 \times 10^{-4}$ J/mol·K^4 and $\delta = 4.4 \times 10^{-6}$ J/mol·K^6. The value of β allows estimating the Debye temperature $\Theta_D = 360$ K for $BaTiSi_2O_7$. This value is similar to the Debye temperature in the Han purple compound $BaCuSi_2O_6$, which amounts to 350 K.[9]

VIII. ELECTRONIC STRUCTURE CALCULATIONS

The experimental results presented above indicate that the magnetic properties of $BaVSi_2O_7$ can be explained within the weakly interacting dimer model. To check this scenario we have performed the electronic structure calculations by using the linear muffin-tin orbital atomic-sphere approximation method with local density approximation (LDA).[15] The band structure obtained and partial densities of states are shown in Fig. 9. There are two well-separated bands, with bonding and antibonding near the Fermi level. According to the partial densities of states presented in Fig. 9, these bands correspond to $3d$ vanadium states of xy symmetry. The lowest excited states are of yz and xz symmetry. Such a structure of the LDA spectrum is typical for $S = 1/2$ vanadium oxides.[16]

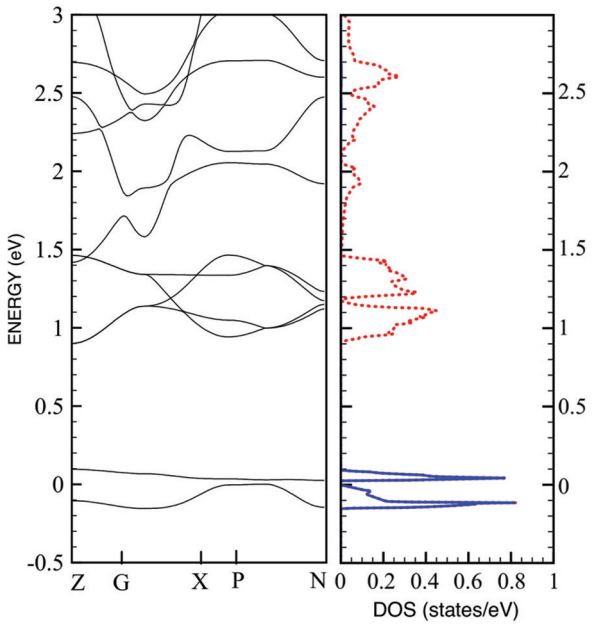

FIG. 9. (Color online) Band structure (left panel) and partial densities of states (right panel) obtained from LDA calculations. The solid and dashed lines are the density of states of $3d$-xy and the total density of $3d$ states, respectively. The Fermi energy corresponds to 0 eV.

It is also interesting to compare the electronic structures of the $BaVSi_2O_7$ and $BaCuSi_2O_6$ compounds. The remarkable difference between them is hybridization strength of transition metal and oxygen states. For the $BaCuSi_2O_6$ system, the ground state (magnetic) e_g orbital of the $x^2 - y^2$ symmetry looks in the direction where the overlap with oxygen is the largest. In the case of $BaVSi_2O_7$, the magnetic t_{2g} orbital is of xy symmetry where lobes point away from the oxygen. Such a difference results in strong superexchange interdimer couplings between magnetic moments in the copper oxide. Moreover, there is a reduction of the magnetic moment of the copper atom that is due to strong hybridization with oxygen.[2]

Another important feature of the electronic spectrum of a transition metal oxide is the energy gap. The LDA calculations (Fig. 9) lead to a gapped state with the splitting of 0.03 eV between bonding and antibonding bands. To reproduce a realistic insulating ground state for $BaVSi_2O_7$, one should take into account Coulomb correlation effects that play an important role in the description of strongly correlated materials. This can be done in the framework of the LDA, taking into account the on-site Coulomb interaction (LDA + U). Such calculations for $BaVSi_2O_7$ reveal an energy gap of 2.4 eV and a magnetic moment of $0.91\mu_B$ associated with vanadium atoms.

Since the exchange interactions between the magnetic moments of vanadium atoms are kinetic in nature, related to the hopping processes, they can be estimated by using the results of the LDA calculations. For these purposes, based on the LDA band structure, we have constructed the low-energy Hamiltonian in the Wannier function basis,

$$H = \sum_{\substack{ij\sigma \\ mm'}} t_{ij}^{mm'} c_{im\sigma}^{+} c_{jm'\sigma}, \tag{11}$$

where i and j are the site indexes, σ denotes spin, $t_{ij}^{mm'}$ is the effective hopping integral that can be calculated by the projection procedure,[17] and $m,m' = xy,yz,3z^2 - r^2,xz, x^2 - y^2$.

Let us first analyze the hopping integrals between the ground state Wannier functions of xy symmetry. The calculated intradimer hopping parameter is equal to −75 meV. The corresponding intradimer exchange interaction parameter can be estimated by using the expression $J_{ij}^{xy} = 4(t_{ij}^{xy})^2/U$, which appears upon mapping the one-band Hubbard model onto the Heisenberg model at the limit $U \gg t$, and which only describes the antiferromagnetic superexchange process. For $U = 5$ eV we obtain $J_d = 4.5$ meV, which is somewhat higher than the experimental estimate of 3.2 meV. The largest interdimer hopping integral of 11 meV is between the upper and bottom sites of neighboring dimers, J_{ac} (Fig. 1, right panel). Since each dimer has eight bonds of this type, the summary interdimer exchange interaction can be calculated as 0.77 meV. Thus, our first principles calculations confirm a weakly interacting dimer model for the magnetic properties of the $BaVSi_2O_7$ system.

The ESR measurements[18] on $BaCuSi_2O_6$ revealed anisotropy effects that can be attributed to a symmetric anisotropic exchange interaction within the spin Hamiltonian

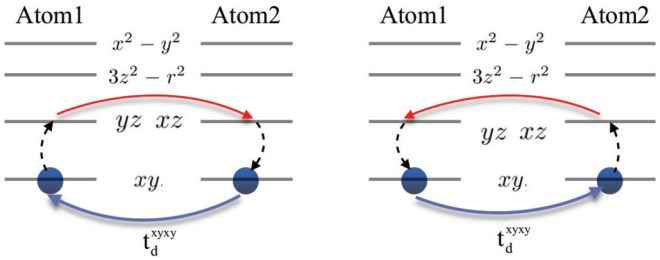

FIG. 10. (Color online) Examples of virtual hopping processes that contribute to the intradimer symmetric anisotropic exchange interactions Γ_d^{xx} and Γ_d^{yy}. Spheres denote the $3d$ electrons that can hop between sites (lower solid lines). The hoppings between empty orbitals are visualized by the upper solid lines. The dashed lines correspond to the mixing of the occupied and empty orbitals due to the spin-orbit coupling.

approach,

$$H_{\text{anis}} = \sum_{\substack{ij \\ \mu\nu}} S_i^{\mu} \Gamma_{ij}^{\mu\nu} S_j^{\nu}, \tag{12}$$

where $\mu, \nu = x, y, z$. Since the atomic structure of $BaCuSi_2O_6$ is close to $BaVSi_2O_7$, one would expect that the vanadium oxide also demonstrates an analogous spin-orbit coupling effect.

We have calculated the symmetric anisotropic exchange interaction tensor $\Gamma_{ij}^{\mu\nu}$ by using a general expression proposed in Ref. 19. It can be derived in the fourth order of perturbation theory with respect to the spin-orbit coupling and transfer integrals. The expression contains all the virtual excitations between Wannier functions centered on $3d$ atomic orbitals of two vanadium atoms (Fig. 10). The intradimer hopping matrix is diagonal—$t_{ij}^{yzyz} = t_{ij}^{xzxz} = 60$ meV, $t_{ij}^{x^2-y^2} = -85$ meV, and $t_{ij}^{3z^2-r^2} = 384$ meV—which means the symmetric anisotropic exchange tensor is also diagonal:

$$\Gamma_{ij}^{xx} = \frac{\lambda^2}{2U}\left(t_{ij}^{xyxy}\frac{\langle xy|L^x|xz\rangle}{\varepsilon_{xz}-\varepsilon_{xy}}t_{ji}^{xzxz}\frac{\langle xz|L^x|xy\rangle}{\varepsilon_{xz}-\varepsilon_{xy}} + \frac{\langle xy|L^x|xz\rangle}{\varepsilon_{xz}-\varepsilon_{xy}}t_{ij}^{xzxz}\frac{\langle xz|L^x|xy\rangle}{\varepsilon_{xz}-\varepsilon_{xy}}t_{ji}^{xyxy}\right),$$

$$\Gamma_{ij}^{yy} = \frac{\lambda^2}{2U}\left(t_{ij}^{xyxy}\frac{\langle xy|L^y|yz\rangle}{\varepsilon_{yz}-\varepsilon_{xy}}t_{ji}^{yzyz}\frac{\langle yz|L^y|xy\rangle}{\varepsilon_{yz}-\varepsilon_{xy}} + \frac{\langle xy|L^y|yz\rangle}{\varepsilon_{yz}-\varepsilon_{xy}}t_{ij}^{yzyz}\frac{\langle yz|L^y|xy\rangle}{\varepsilon_{yz}-\varepsilon_{xy}}t_{ji}^{xyxy}\right),$$

and

$$\Gamma_{ij}^{zz} = \frac{\lambda^2}{2U}\left(t_{ij}^{xyxy}\frac{\langle xy|L^z|x^2-y^2\rangle}{\varepsilon_{x^2-y^2}-\varepsilon_{xy}}t_{ji}^{x^2-y^2}\frac{\langle x^2-y^2|L^z|xy\rangle}{\varepsilon_{x^2-y^2}-\varepsilon_{xy}} + \frac{\langle xy|L^z|x^2-y^2\rangle}{\varepsilon_{x^2-y^2}-\varepsilon_{xy}}t_{ij}^{x^2-y^2}\frac{\langle x^2-y^2|L^z|xy\rangle}{\varepsilon_{x^2-y^2}-\varepsilon_{xy}}t_{ji}^{xyxy}\right). \tag{13}$$

Here λ is the spin-orbit coupling constant, $\langle m'|\dot{L}|m\rangle$ is a matrix element of orbital magnetic moment operator, and ε_m is the energy of the Wannier orbital. Using $\lambda = 60$ meV, $U = 5$ eV, and the energies of the Wannier orbitals presented in Table I we obtain $\Gamma_d^{xx} = \Gamma_d^{yy} = 0.002$ meV and $\Gamma_d^{zz} = -0.003$ meV.

Thus the intersite anisotropy can be estimated as 0.06 K, which is two times smaller than that observed in the corresponding copper oxide, $BaCuSi_2O_6$. In principle one can estimate such anisotropy from the ESR experiments. However, in our case, the lowest experimentally available temperature of 6 K is still too high to observe such a tiny effect. We hence leave the experimental confirmation of this theoretical prediction for future investigations.

IX. CONCLUSION

The "e_g orbital" counterpart of the V-based silicate, i.e., $BaCuSi_2O_6$, has attracted significant attention in view of Bose–Einstein condensation of magnons in this dimer system. Against this background it is intriguing to understand similarities and discrepancies in the "t_{2g} orbital" counterpart, $BaVSi_2O_7$. As in the Cu-system, a variety of sophisticated experiments are needed to fully elucidate the excitation spectra and magnetic field effects at presumably ultralow temperatures and with single crystals. However, the work at hand provides a valuable starting point because it is important to establish its basic properties, i.e., scale of intradimer and interdimer exchange interactions, etc. In the present study, the $S = 1/2$ dimer system $BaVSi_2O_7$ is characterized by means of thermodynamic and resonant measurements. The broad maximum in the temperature dependence of the magnetic susceptibility and a Schottky-type anomaly in the specific heat allows estimation of the main exchange interaction within V^{4+}-V^{4+} dimers as $J = 37 \pm 1$ K. This estimation is corroborated by pulsed magnetic field measurements, which is evidenced by the field-induced singlet-triplet transition at about 27 T. The interdimer exchange interaction is estimated to be significantly smaller compared with the intradimer exchange interaction. The temperature dependences of the ESR X-band intensity, as well as that in the terahertz regime, are in good correspondence with the thermodynamic measurements. The electronic structure calculations with the use of LDA indicate that the magnetic properties of $BaVSi_2O_7$ can be explained within the weakly interacting dimer model. Contrary to the strongly interacting e_g dimer system $BaCuSi_2O_6$, its t_{2g} counterpart $BaVSi_2O_7$ demonstrates features of nearly isolated dimers.

ACKNOWLEDGMENTS

This work has been supported by the grant program of the President of the Russian Federation MK-5565.2013.2, MK-7138.2013.2; Russian Foundation for Basic Research Grants 11-02-00083, 12-02-90823, 12-02-90924, 12-02-90810, 12-02-31331, 13-02-00174; and the contracts of the Ministry of education and science of Russia N 14.A18.21.0076 and 14.A18.21.0889. A.V. and O.V. acknowledge visiting grants support from the International Collaboration Center Institute for Materials Research of Tohoku University.

[1] J. Deisenhofer, R. M. Eremina, A. Pimenov, T. Gavrilova, H. Berger, M. Johnsson, P. Lemmens, H.-A. Krug von Nidda, A. Loidl, K.-S. Lee, and M.-H. Whangbo, Phys. Rev. B **74**, 174421 (2006).

[2] S. Taniguchi, T. Nishikawa, Y. Yasui, Y. Kobayashi, M. Sato, T. Nishioka, M. Kontani, and K. Sano, J. Phys. Soc. Jpn. **64**, 2758 (1995).

[3] A. W. Garrett, S. E. Nagler, D. A. Tennant, B. C. Sales, and T. Barnes, Phys. Rev. Lett. **79**, 745 (1997).

[4] E. Dagotto and T. M. Rice, Science **271**, 618 (1996).

[5] S. Notbohm, P. Ribeiro, B. Lake, D. A. Tennant, K. P. Schmidt, G. S. Uhrig, C. Hess, R. Klingeler, G. Behr, B. Büchner, M. Reehuis, R. I. Bewley, C. D. Frost, P. Manuel, and R. S. Eccleston, Phys. Rev. Lett. **98**, 027403 (2007).

[6] H. Kageyama, K. Yoshimura, R. Stern, N. V. Mushnikov, K. Onizuka, M. Kato, K. Kosuge, C. P. Slichter, T. Goto, and Y. Ueda, Phys. Rev. Lett. **82**, 3168 (1999).

[7] O. Volkova, I. Morozov, V. Shutov, E. Lapsheva, P. Sindzingre, O. Cepas, M. Yehia, V. Kataev, R. Klingeler, B. Büchner, and A. Vasiliev, Phys. Rev. B **82**, 054413 (2010).

[8] H. Nojiri, H. Kageyama, K. Onizuka, Y. Ueda, and M. Motokawa, J. Phys. Soc. Jpn. **68**, 2906 (1999).

[9] M. Jaime, V. F. Correa, N. Harrison, C. D. Batista, N. Kawashima, Y. Kazuma, G. A. Jorge, R. Stein, I. Heinmaa, S. A. Zvyagin, Y. Sasago, and K. Uchinokura, Phys. Rev. Lett. **93**, 087203 (2004).

[10] G. Liu and G. E. Greedan, J. Solid State Chem. **108**, 267 (1994).

[11] H. Nojiri, M. Motokawa, K. Okuda, H. Kageyama, Y. Ueda, and H. Tanaka, J. Phys. Soc. Jpn. Suppl. B **72**, 109 (2003).

[12] G. A. Bain and J. F. Berry, J. Chem. Education **85**, 532 (2008).

[13] Y.-J. Liu, J. A. Cowen, T. A. Kaplan, D. C. DeGroot, J. Schindler, C. R. Kannewurf, and M. G. Kanatzidis, Chem. Mater. **7**, 1616 (1995).

[14] R. Klingeler, B. Büchner, K.-Y. Choi, V. Kataev, U. Ammerahl, A. Revcolevschi, and J. Schnack, Phys. Rev. B **73**, 014426 (2006).

[15] O. K. Andersen, Phys. Rev. B **12**, 3060 (1975); O. K. Andersen and O. Jepsen, Phys. Rev. Lett. **53**, 2571 (1984).

[16] M. A. Korotin, I. S. Elfimov, V. I. Anisimov, M. Troyer, and D. I. Khomskii, Phys. Rev. Lett. **83**, 1387 (1999).

[17] V. I. Anisimov, D. E. Kondakov, A. V. Kozhevnikov, I. A. Nekrasov, Z. V. Pchelkina, J. W. Allen, S.-K. Mo, H.-D. Kim, P. Metcalf, S. Suga, A. Sekiyama, G. Keller, I. Leonov, X. Ren, and D. Vollhardt, Phys. Rev. B **71**, 125119 (2005).

[18] S. A. Zvyagin, J. Wosnitza, J. Krzystek, R. Stern, M. Jaime, Y. Sasago, and K. Uchinokura, Phys. Rev. B **73**, 094446 (2006).

[19] M. V. Eremin, D. V. Zakharov, R. M. Eremina, J. Deisenhofer, H.-A. Krug von Nidda, G. Obermeier, S. Horn, and A. Loidl, Phys. Rev. Lett. **96**, 027209 (2006).